This is a repository copy of *Temperature-dependent structure and dynamics of highly-branched poly(N-isopropylacrylamide) in aqueous solution*.

White Rose Research Online URL for this paper:
http://eprints.whiterose.ac.uk/128118/

Version: Accepted Version

Article:

Soft Matter

ARTICLE

Temperature-dependent structure and dynamics of highly-branched poly(*N*-isopropylacrylamide) in aqueous solution

Ateyyah M. AL-Baradi,[a,b] Stephen Rimmer,[c, §] Steven R. Carter,[a,c] Johann P. de Silva,[d] Stephen M. King,[e] Marco Maccarini,[f, †] Bela Farago,[f] Laurence Noirez,[g] and Mark Geoghegan [a,*]

Small-angle neutron scattering (SANS) and neutron spin-echo (NSE) have been used to investigate the temperature-dependent solution behaviour of highly-branched poly(*N*-isopropylacrylamide) (HB-PNIPAM). SANS experiments have shown that water is a good solvent for both HB-PNIPAM and a linear PNIPAM control at low temperatures where the small angle scattering is described by a single correlation length model. Increasing the temperature leads to a gradual collapse of HB-PNIPAM until above the lower critical solution temperature (LCST), at which point aggregate occurs, forming disperse spherical particles of up to 60 nm in diameter, independent of the degree of branching. However, SANS from linear PNIPAM above the LCST is described by a model that combines particulate structure and a contribution from solvated chains. NSE was used to study the internal and translational solution dynamics of HB-PNIPAM chains below the LCST. Internal HB-PNIPAM dynamics is described well by the Rouse model for non-entangled chains.

Introduction

Hyperbranched polymers are an important class of material because the large chain-end density permits a level of functionalization inaccessible in other classes of polymers[1-7] as well as control over many physical properties.[6] Furthermore, they have unusual rheological properties because they do not entangle in solution, which means that they tend to have low viscosity compared to linear polymers at the same concentration.[3, 5] They also have enhanced solubility compared to dendrimers of similar molar mass which is evident by their larger sizes,[8] and can be synthesized on a much larger scale.[9]

[a.] *Department of Physics and Astronomy, Hounsfield Road, University of Sheffield, Sheffield S3 7RH, UK.*
[b.] *Department of Physics, Taif University, Taif 888, Saudi Arabia.*
[c.] *Department of Chemistry, Brook Hill, University of Sheffield, Sheffield S3 7HF, UK.*
[d.] *Laboratoire de Physique des Solides-UMR 8502-Université Paris-Sud, F-91405 Orsay, France.*
[e.] *ISIS Pulsed Neutron and Muon Facility, Rutherford Appleton Laboratory, Chilton, Didcot, Oxon OX11 0QX, UK.*
[f.] *Institut Laue-Langevin, 71 avenue des Martyrs, F-38000 Grenoble, France.*
[g.] *Laboratoire León Brillouin CEA-CNRS, Saclay, F-91191 Gif-sur-Yvette Cedex, France.*

§ *Present address: School of Chemistry and Forensic Sciences, Richmond Building, University of Bradford, Bradford BD7 1DP, UK; s.rimmer@bradford.ac.uk.*

† *Present address: Equipe SyNaBi, Université Grenoble Alpes, Laboratoire TIMC-IMAG UMR CNRS 5525, Pavillon Taillefer, Domaine de la Merci, 38700 La Tronche, France.*

* mark.geoghegan@sheffield.ac.uk.

Electronic Supplementary Information (ESI) available: [Tables of quantities of materials used in synthesis, NMR characterization spectra, GPC characterization data, rheology characterization data, confocal microscopy images, further SANS and NSE analysis, and tables of results]. See DOI: 10.1039/x0xx00000x

The structure of hyperbranched polymers is expected to be globular. Dendrimers are spherical due to the order inherent in their structure, but hyperbranched materials are less controlled in structure and can generally be treated as fractals.[10-12] However, the fractal dimension of hyperbranched polymers must reflect the solubility of that polymer. In a poor solvent, the polymers collapse and aggregate, with an associated increase in fractal dimension.

Highly-branched polymers cannot entangle because the large number of branching points results in arms that are too short to combine with those from a neighbouring molecule. Although entanglement is not possible, the interaction between polymer and solvent is critical because in poor solvents aggregation can be observed.[13]

Hyperbranched polymers can be expected to exhibit local Rouse dynamics, although whether there are significant hydrodynamic effects has not been the subject of extensive work. Relaxation of these polymers close to the glass transition has been given some attention because of the dramatic effect that the end group has on these processes.[14, 15] Nevertheless, even in dilute solution, branches are in a crowded environment and so their dynamics will be affected by their neighbours.

In addition to the density of functional groups available to hyperbranched polymers, the capacity of some polymers to respond to their environment (e.g. temperature, pH, or salt) gives rise to 'smart' behaviour appropriate for new technologies involving controlled release or actuation.[16] The temperature-sensitive polymer, poly(*N*-isopropylacrylamide) (PNIPAM) is a particularly good example of an environmentally responsive polymer because of its temperature-induced coil-globule transition at 32°C, above which it collapses due to

intra-chain hydrogen bonding.[17] Grafting PNIPAM to different surfaces has, for example, allowed excellent control of cell detachment[18-22] and the application of biocidal properties.[23] This capability is readily available with branched PNIPAM,[24] but the ability to functionalize the end groups allows the ability to sense specific bacteria.[25]

The large number of functional groups in hyperbranched polymers is controlled by the density of branching points. In this work, PNIPAM has been synthesized with three different branching ratios by a self-condensing vinyl polymerization route and its structure has been determined by small-angle neutron scattering (SANS) both above and below its lower critical solution temperature (LCST). These data confirm that the polymers are fractal objects below the LCST, but above it the polymers form spherical aggregates with a commensurate increase in fractal dimension. Dynamical properties below the LCST were obtained using neutron spin-echo (NSE), which show that Rouse dynamics describe local motion. It was also possible to obtain translational diffusion coefficients using NSE, which were found to be comparable to those of a different polymer with similar structure.

Table 1. GPC results for polymer weight average molar masses and dispersities

NIPAM/RAFT feed ratio	PNIPAM		D7-PNIPAM	
	M_w (kDa)	dispersity	M_w (kDa)	dispersity
(25:1)	316	17	367	17
(60:1)	169	5.3		
(90:1)	357	9.6	190	4.0
Linear	136	2.1		

Experimental

Synthesis overview.

Highly-branched poly(*N*-isopropylacrylamide) (HB-PNIPAM) was synthesized using a RAFT branching agent, as previously described.[26] The resultant highly-branched polymers contained the residual *N*-pyrrole dithioate RAFT groups at their chain-ends and these were converted to carboxylic acid chain-end functionalized polymers using a previously developed methodology.[27] Three HB-PNIPAM samples with different degrees of branching (number of monomers between branch points) were synthesized.

Synthesis of highly-branched *N*-pyrrole chain-end-functionalized poly(*N*-isopropylacrylamide).

N-isopropylacrylamide (NIPAM), 4-vinylbenzylpyrrolecarbodithioate (RAFT agent, which also causes branching), and azobis(isobutyronitrile) (AIBN, initiator) were dissolved in dioxane (quantities are given in **Table S1**).

The mixture was then transferred to a glass ampoule. Three freeze-pump thaw cycles were carried out at 10^6 Pa before the ampoule was sealed. It was then heated at 60 °C for 48 h and quenched with liquid nitrogen. The polymer solution (**Scheme 1**) was precipitated by dropwise addition to diethylether (600 ml). The ether was decanted off and the solids were further washed with ether, and then dried at room temperature in a vacuum oven for 16 h. The procedure was repeated twice more to give a yellow solid (yields are listed in **Table S1**). For NSE experiments, where partially deuterated NIPAM was used, the same synthesis was performed with the same masses of D7-NIPAM as those in **Table S1**. This caused a small change in the NIPAM/RAFT ratio due to the different densities of NIPAM and D7-NIPAM; the partially deuterated NIPAM contains seven deuterons on the isopropylacrylamide moiety, i.e. $O=C(ND)C(CD_3)_2$.

Scheme 1. Synthesis of *N*-pyrrole chain-end-functionalized poly(*N*-isopropylacrylamide)

The polymers were characterized by gel permeation chromatography (GPC) in oxolane (tetrahydrofuran) using a triple detector with 0.1% tetrabutyl-ammonium bromide as eluent. The measurements were made using PL gel (two mixed C) columns with a flow rate of 1.0 mL/min. The weighted average molar masses and dispersities obtained from these experiments are presented in **Table 1**. The large dispersities obtained are typical of this route to HB-PNIPAM.[26] Some GPC data are shown in **Figure S2** of the supporting information.

A Bruker 400 MHz NMR spectrometer was used to obtain NMR spectra for HB-PNIPAM at room temperature. 70 mg of each polymer was dissolved in 1 ml of deuterated chloroform and then transferred to an NMR tube. NMR spectra were used to calculate the actual branching degrees, as shown in **Table 2**, which is the ratio of NIPAM to imidazole obtained from the integration of NMR spectra. In what follows the feed ratio is used to identify the branching ratios, because this is consistent across the different HB-PNIPAM.

Table 2. Branching ratios after conversion of *N*-pyrroledithioate (chain end) highly-branched polymers to carboxylic acid (chain end) functionalized polymers

NIPAM/RAFT feed ratio	Measured branching ratio PNIPAM	Measured branching ratio D7-PNIPAM
(25:1)	48:1	21:1
(60:1)	82:1	57:1
(90:1)	94:1	78:1

Scheme 2. Synthesis of *carboxylic acid chain end functionalized poly(N-isopropylacrylamide)*

Synthesis of highly-branched carboxylic acid chain end functionalized poly(*N*-isopropylacrylamide).

The highly-branched *N*-pyrroledithioate chain-end polymers described above were dissolved in DMF (degassed with nitrogen for 30 min) and stirred at 60°C under a nitrogen atmosphere. 4,4'-azobis-(4-cyanopentanoic acid) was added to the reaction mixture as a solution in DMF (20 equivalents relative to the number of pyrrole chain-end groups) and heated at 60°C for 16 h (**Scheme 2**). This procedure was repeated twice more so that a total of 60 equivalents of the reagent were added. The DMF was removed under high vacuum at 40-50°C and the resultant oil ultra-filtered using a blend of acetone/ethanol (10:1 by volume) through a cellulose filter (3 kDa cut-off). The resultant concentrate was evaporated under reduced pressure and dried under vacuum at room temperature to give a buff-coloured solid. The quantities and yield of this reaction are shown in **Table S2**.

Synthesis of linear PNIPAM.

Synthesis of linear PNIPAM was achieved using the same methodology for the hyperbranched polymer but with the 4-vinylbenzylpyrrolecarbodithioate RAFT agent replaced by benzylpyrrolecarbodithioate.

Determination of lower critical solution temperature.

A Cary 3Bio UV-visible spectrophotometer, fitted with a Cary temperature controller, was used to determine the LCST of different concentrations (5 mg/ml and 10 mg/ml) of PNIPAM and carboxylic acid-terminated HB-PNIPAMs in D_2O. A Varian Cary temperature controller was used to control the temperature of the cell holder to an accuracy of 0.1 °C, and condensation onto the sample cell holder was avoided by a flow of nitrogen gas. All samples were heated from 15 °C to 60 °C at 2 °C/min and the LCST obtained using a wavelength of 500 nm. The LCST of the polymer was determined as the point of inflexion of the increased absorbance with increasing the temperature and the results are summarized in **Table 3**.

Table 3. PNIPAM LCST in D_2O

PNIPAM sample	LCST (5% polymer) / °C	LCST (9% polymer) / °C	LCST (D7-PNIPAM, 4% polymer) / °C
HB (25:1)	26	25	28
HB (60:1)	24	24	
HB (90:1)	30	18	30
linear	32	32	

Small-angle neutron scattering.

SANS measurements were performed at the Rutherford Appleton Laboratory using the fixed-geometry, time-of-flight LOQ diffractometer[28] on the ISIS Spallation Neutron Source, and at the Laboratoire Léon Brillouin using the PAXY instrument on the Orphée reactor. Both instruments were equipped with two-dimensional detectors. At ISIS, the LOQ instrument uses incident neutron wavelengths from λ = 2.2 to 10.0 Å, which covers a range of scattering wave vector (magnitude) of Q = 0.009 to 1.3 Å^{-1} at a sample-detector distance of 4.1 m. 5% and 9% solutions by mass of each polymer ((25:1), (60:1), and (90:1) HB-PNIPAM and linear PNIPAM) were prepared by dissolving 150 and 300 mg respectively in 2.8 ml of D_2O. All samples were transferred to 2 mm path-length quartz Hellma cells. The temperature was controlled using circulating fluid baths. A similar procedure was used on the PAXY instrument which covers almost a similar Q-range, from 0.003 to 1 Å^{-1}, using a sample-detector distance of 1.1 (λ = 5 Å) to 7 m (λ = 6 and 12 Å). The wavelength resolution on PAXY was kept to $\lambda/\Delta\lambda$ = 0.14±0.01. Scattering intensities were reduced as described previously,[29] using the software provided by each facility to obtain the differential scattering cross section, $d\Sigma/d\Omega$, in absolute units (cm^{-1}), which is referred to here as $I(Q)$.

Neutron spin-echo.

NSE measurements were carried out using the IN15 spectrometer at the Institut Laue-Langevin[30] with an incident beam wavelength of 10 Å and $\Delta\lambda/\lambda$ = 0.15. With these settings, the maximum spin-echo time achievable was 50.5 ns. By changing the detector angle, the momentum transfer (divided by $\hbar$) spanned 0.0438 Å^{-1} ≤ Q ≤ 0.1524 Å^{-1}. 4% w/w solutions of two different D7-HB-PNIPAM, (25:1) and (90:1), were prepared by dissolving 150 mg of each polymer in 3 ml D_2O. The samples were held in a 2 mm path length aluminium cell
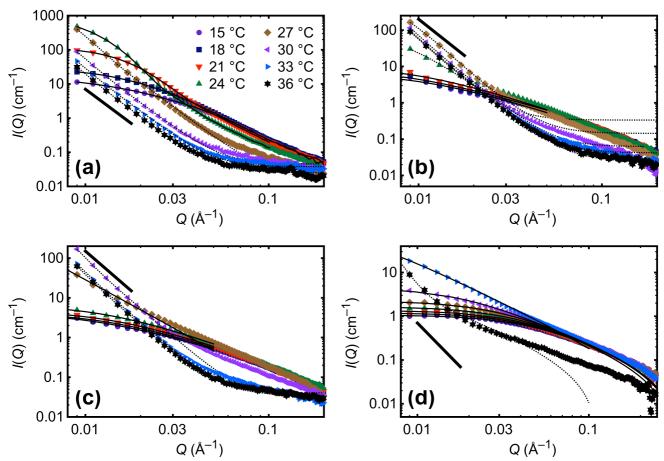
Figure 1. Double-logarithmic plots of SANS data (background-subtracted) as a function of the magnitude of the scattering vector for 5 wt% of (a) HB-PNIPAM (25:1), (b) HB-PNIPAM (60:1), (c) HB-PNIPAM (90:1) and (d) linear PNIPAM in D_2O at temperatures below and above their LCSTs. Broken lines in (a), (b), and (c) are fits to a disperse spherical structure (**eqn 3**). This structure exhibits Porod behaviour at low Q. The thick solid curves represent a power-law exponent of −4 to correspond to Porod behaviour. These fits are only applied to data for samples at or above the LCST. Full lines in (a), (b), (c), and (d) are fits to **eqn (1)**, and correspond to samples below the LCST. The broken line in (d) is a fit to **eqn (2)**

(4 × 3 mm). NSE measurements were conducted at 15 °C and 25.4 °C for D7-HB-PNIPAM (25:1), and at 24 °C and 31.1 °C for D7-HB-PNIPAM (90:1). These temperatures are well below and close to the LCST of the respective polymers. All NSE spectra were corrected and background subtracted from the scattering of the pure solvent and the sample holder.

Structure of highly-branched PNIPAM

Temperature dependence.

Figure 1 shows double logarithmic plots of SANS data from HB-PNIPAM (5 wt% in D_2O) with different branching degrees, and the data for the linear PNIPAM control. Below the LCST, the scattering intensity increases with increasing temperature in both cases at low Q, but above the LCST the scattering intensity decreases with increasing temperature. The former behaviour is well established in related systems,[31] whilst the latter is more unusual.

The structure of the highly-branched polymers is best revealed by Kratky plots, i.e. $I(Q)Q^2$, where $I(Q)$ is the background subtracted intensity. These are in **Figure 2**. At the lowest temperatures, for both the linear and highly-branched polymers, the Kratky plots reveal an increase in intensity with increasing Q, followed by a plateau at large Q. This behaviour

indicates a random solvated coil. As the temperature is increased and the polymer starts to collapse a (correlation) peak is observed at $Q = Q_{max}$, with Q_{max} decreasing with increasing temperature. For the most-branched polymer, below the LCST (**Figure 2a**), the correlation peak corresponds to length scales of 20 to 72 nm (i.e. $\sqrt{6}/Q_{max}$) between 15 and 21°C. These maxima in the Kratky plots indicate non-randomly branched structures in solution.[32, 33] Compact (but solvated) hyperbranched polyglycerols[13] and polyesters[34] also exhibited the peak in the Kratky representation, which is absent from linear polymers.[35] These maxima disappear at temperatures above the LCST because the scattering at this Q-range represents the overall globular structure of the collapsed HB-PNIPAM. In the case of the PNIPAM studied here, there is also a difference in the behaviour of the linear polymers above and below the LCST (**Figure 2d**). A similar scattering behaviour was observed from less branched PNIPAM (60:1) and (90:1), shown in **Figures 2b** and **2c**, respectively, above their LCSTs. However, the correlation peak observed below the LCST of the (25:1) sample is absent for these less crosslinked samples, and this absence can be attributed to the larger distances between branches, which is likely to force the peak to smaller Q than accessed here. That there is a difference in HB-PNIPAM structure above and below the LCST is worth noting, because
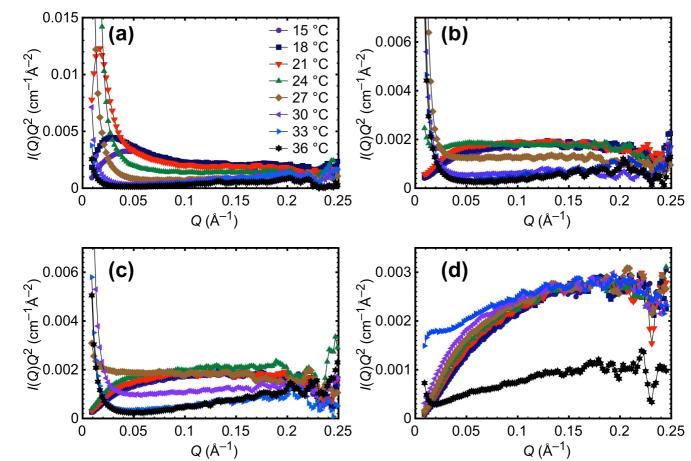
Figure 2. Temperature dependent evolution of the (background-subtracted) SANS scattering profiles represented as Kratky plots of 5 wt% for (a) HB-PNIPAM (25:1), (b) (60:1), (c) (90:1), and (d) linear PNIPAM in D$_2$O. The solid lines are guides for the eye

one could consider the branched units on HB-PNIPAM as analogues of dilute or small PNIPAM brush layers,[36, 37] or small arms of PNIPAM bottle brushes[31] which have been shown not to undergo significant collapse transitions.

It is clear from the data presented in **Figure 1** that the scattering from linear and HB-PNIPAM below the LCST, when they are completely swollen in D$_2$O, is different from that above it, when they are collapsed. The change of gradient in the scattering data suggests scattering from objects with different fractal dimension, D_f, due to the temperature-dependent change in polymer conformation. This means that the scattering intensity decays with a power law depending on Q^{D_f}, where D_f correlates mass and size (R) by $M \propto R^{D_f}$, which according to Flory theory is given by $D_f = 5/3$ for linear polymers[38] and $D_f = 2$ for branched polymers[39] in a good solvent. The scattering function in this case is given by the generalized Zimm equation,

$$I(Q) = \frac{I_0}{\left(1 + \frac{\left(1 + D_f\right)\xi^2 Q^2}{3}\right)^{D_f/2}}, \qquad (1)$$

where I_0 is a constant and ξ is a correlation length. This equation collapses to the standard Ornstein-Zernike formalism when $D_f = 2$. The scattering from linear PNIPAM (**Figure 1d**) below the LCST is described well by **eqn (1)** with a fractal dimension $D_f = 5/3$ which does not change with increasing

temperature until the LCST is reached. The correlation length, ξ increases slightly with increasing temperature. **Figure 3a** summarizes the values of ξ obtained by fitting to the generalized Zimm equation (**eqn 1**) for the 5% samples. Even above the LCST, SANS data for linear PNIPAM are described by **eqn (1)**, but the fractal dimension increases to 1.9 and the correlation length increases significantly as well. This fractal dimension remains close to that for a polymer random walk but the rapidly increasing correlation length is due to an increasing contribution from inter-chain interactions creating separated particles.

It is noteworthy that $D_f = 4$ at temperatures below the LCSTs of HB-PNIPAM (25:1) and (60:1), which means that the polymers may be considered well-defined separated three-dimensional objects.[11, 40, 41] However, this result was not seen in the case of the least branched PNIPAM (90:1) below its LCST (30°C) where D$_2$O was (from the fractal dimension result) a neutral solvent up to a temperature close to the LCST. The correlation length in **Figure 3** shows a decrease in ξ with temperature for all HB-PNIPAMs, confirming the gradual collapse of these polymers below their LCSTs. This change in correlation length (also observed in the 9% samples) allows the possibility that the behaviour of the HB-PNIPAM as the LCST is approached from below is somewhat similar to gelation, although in that case $D_f = 6$ can be expected, which is not observed here.[42]
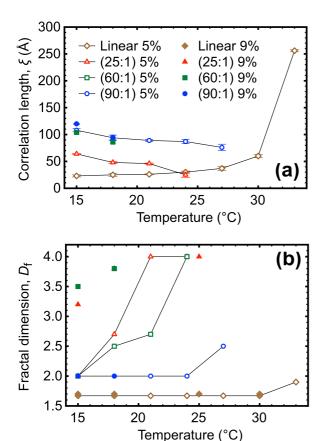
Figure 3. Temperature-dependent evolution of the correlation length (a) and fractal dimension (b) for the 5% and 9% by mass linear and HB-PNIPAM samples obtained from fitting the SANS data for samples below the LCST to **eqn (1)**. For the 5% samples (a) some symbols are obscured so D_f = 2 for all HB-PNIPAM at 15°C; D_f = 4 for the (25:1) and (60:1) HB-PNIPAM samples at 24 °C; and Df = 1.7 for the linear PNIPAM at 15, 18, and 30 °C. The legend spans both graphs

Scattering from linear PNIPAM at 36 °C (well above its LCST) in Figure 1d shows a different behaviour from that below its LCST. The gradient of the intensity in this case, as shown in the double logarithmic plot in **Figure 1d**, indicates behaviour close to the Porod regime with a slope close to –4 at the smallest Q. The deviation from Porod behaviour is attributed to the contribution of Lorentzian scattering resulting from the slightly solvated and entangled polymer chains. SANS data in this case is better described by a model that combines Porod and Lorentzian scattering,[43] given by

$$I(Q) = \frac{6\pi\phi(\Delta\rho)^2}{Q^4 r_0}\left(1 + \frac{1}{Q^2 r_0^2}\right) + \frac{I_L}{\left(1 + \xi^2 Q^2\right)}, \qquad (2)$$

where r_0 is the particle radius, ϕ is the particle volume fraction, and I_L is a constant. This equation has also previously been applied to microgels of PNIPAM.[44] The first term in **eqn (2)** corresponds to Porod behaviour for scattering from the whole particle, from which the shape and size of the polymer can be obtained. The second term in this equation is the Lorentzian scattering contribution from the internal structure of the polymer, from which the interactions with other chains can be determined through the correlation length. A coupling term was not used here. Fitting the SANS data for linear PNIPAM at 36 °C to the Porod-Lorentzian model (**eqn 2**), gives an effective
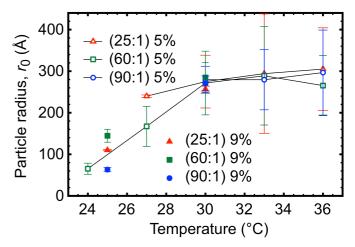

Figure 4. Temperature-dependent evolution of the particle radius, r_0, obtained by fitting SANS data for 5 and 9 wt% HB-PNIPAMs in D_2O above their LCST to scattering from disperse spheres. For the 5 wt% linear PNIPAM, the combined function (**eqn 2**) was used, and then only at 36 °C to give r_0 = 0.127±0.004 µm (not shown)

particle radius (r_0 = 127 nm), indicating aggregated rather than individual molecules. (Although it is reasonable to note the increase in size, the quality of the fit is not good enough to be confident in the length scale, particularly given the rather large size of the particles.) This scattering behaviour of linear PNIPAM above its LCST is attributed to the entanglements and polymer-polymer interactions formed when the polymer collapses with increasing temperature. A similar behaviour to the scattering from linear PNIPAM above 32°C was observed in the case of collapsed microgels, for which SANS data were also fitted to **eqn (2)**.[44]

Above the LCST, the SANS of both linear and HB-PNIPAMs exhibits a Q^{-1} tail at high Q values which is independent of temperature and not captured in **eqn (2)**. As this arises from shorter length scales it most likely originates from the (more rigid local) internal structure, such as from the backbone between branches in the case of HB-PNIPAM, which would in turn mean that the branches and their COOH end-groups play a significant role in controlling the overall shape and size of HB-PNIPAMs as the internal structure is similar to that of linear PNIPAM.

Although fitting the data for the HB-PNIPAM samples above the LCST to Porod behaviour (the first term in **eqn 2**) gives good results (see **Figure S5** of the **ESI**), a more accurate understanding of the behavior of the HB-PNIPAM can be obtained by considering dispersity in the particle size. Here the scattering function is given by

$$I(Q) =$$

$$\int_0^\infty \left(\frac{16\pi^2 r_m}{9K_n \sigma r}\exp\left(\frac{-1}{2}\left(\frac{r_m \ln(r/r_m)}{\sigma}\right)^2\right)\right)r^6\left(\frac{\sin(Qr) - Qr\cos(Qr)}{(Qr)^3}\right)^2 dr \quad (3)$$
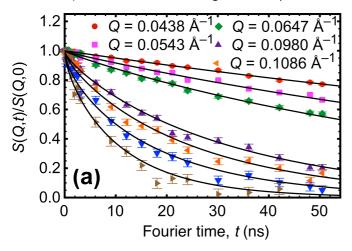
where the first bracketed term in the integral is the particle size distribution function, for which K_n is a normalization factor, r_m is the mean radius of the spheres so that σ/r_m represents the dispersity. These fits are included in **Figure 1** for the hyperbranched polymers. It can be seen in **Figure 1** that the gradient at small Q is slightly greater than expected from

Porod behaviour, which has also been observed for PNIPAM microgels[45] and explained as being due to surface fractals on the spherical particles.[46]

The particle sizes increase with increasing temperature (see **Figure 4**), although the size does not change much at the highest temperatures measured. The 5% HB-PNIPAM particles were disperse with the dispersity limited by $0.34 < \sigma/r_m < 0.45$. The range of dispersity was considerably greater for the 9% HB-PNIPAM particles. However, particle size seems to be independent of the degree of branching as all HB-PNIPAMs in this study showed, within errors, similar average particle radii (~280 Å at or above 30°C). Given the relatively large size of these particles it is likely that they are aggregates, but they are defined in size, even if they are rather disperse. This indicates that, at least on the time scales of the experiments, the HB-PNIPAM is not fully coalescing above the LCST.

Concentration dependence.

In general, scattering from 9 wt% HB-PNIPAM exhibits similar behaviour to that at the lower concentration insofar as the data were fitted to **eqn (1)** below the LCST and to a Porod scattering function around the LCST (**Figure S5** in supporting information). Both the correlation length and the particle size
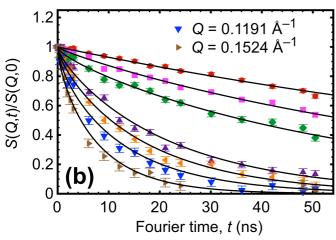
(**Figure 4**, obtained from fitting the SANS data to **eqn 3**) are largely independent of concentration. The fractal dimension, D_f, increases with increasing concentration below the LCST of HB-PNIPAMs (25:1) and (60:1) indicating that the quality of D$_2$O as a solvent for HB-PNIPAMs changes with concentration, possibly affecting the internal structure of these polymers but not the overall shape. Scattering from HB-PNIPAMs below the LCST for both high and low concentrations can be considered using **eqn (1)**, which means these HB-PNIPAM chains do not entangle with increasing temperature even at concentrations as high as 9% w/w, which is as expected for hyperbranched polymers.[47]

Dynamics of HB-PNIPAM

NSE data for D7-HB-PNIPAM samples in water are presented in **Figure 5**. These figures show the Fourier time (t)-dependent intermediate scattering function, $S(Q,t)/S(Q,0)$, for the different branching degrees at temperatures below and close to the LCST of each polymer. The intermediate scattering function here comprises a translational term, which describes diffusion, D_0, which is important at small Q, and a term describing internal dynamics for which a stretched exponential is generally appropriate. If Rouse internal dynamics were all that contributed to the data, then a scaling relation could be applied that allows the data for each polymer to collapse onto a single curve.[48] This was not the case, and the (failed) scaling is shown in **Figure S8** in the **ESI**. $S(Q,t)/S(Q,0)$ is then given by[49]

$$\frac{S(Q,t)}{S(Q,0)} = \exp\left(-D_0 Q^2 t\right)\left(A + (1-A)\exp\left(-\left(\Gamma t\right)^\beta\right)\right), \quad (4)$$

where $0 \leq A \leq 1$, and β is a stretching exponent. Γ is an internal relaxation rate, which, for Rouse dynamics, is given by[49]

$$\Gamma = \frac{k_B T b^2 Q^4}{2\zeta}, \quad (5)$$

where k_B is the Boltzmann constant, T is the absolute temperature, ζ is the friction coefficient and b, the step (Kuhn) length (monomer size). The coupling of a translational diffusion with short-scale motion for less complex systems

Figure 5. Intermediate scattering function for D7-HB-PNIPAM (a) (25:1) at 15.0 °C and (b) (90:1) at 24.0 °C in D$_2$O at the values of Q indicated. The LCST of these polymers at the concentration of 4% (w/w) is 28°C and 30°C (**Table 3**). The solid lines are fits to **eqn 4** with $\beta = 1/2$
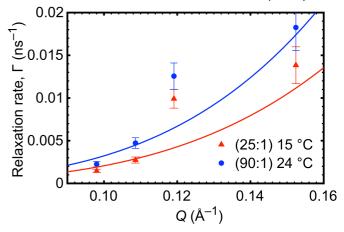
Figure 6. Relaxation rate, Γ, extracted from **eqn 4** of (25:1) and (90:1) D7-HB-PNIPAM as a function of Q. The solid lines represent fits to **eqn 5**

such as vesicles[50] and microemulsions[51] is reasonably well understood and requires $\beta = 1$, which signifies a collective diffusion. Modifying this for polymeric systems involves a different Q-dependence of the local motion. Here the same principle of combining local and translational motion can be used with multiple diffusion coefficients dependent upon the nature of the motion. For microgels, this can mean a particle, the mesh, or local polymer dynamics.[52] For highly-branched polymers, the same considerations may be used, but analysis using D_0 and Γ was sufficient to give good fits to the data.

To fit the data, D_0 was extracted from the data obtained at $Q = 0.0438$ Å^{-1} (the smallest value of Q measured) by forcing $A = 1$ at this Q for fits to **eqn 4**. Holding $A = 1$ presupposes that NSE is solely interrogating diffusive behaviour at this Q, the legitimacy of which was tested by confirming that $A \approx 1$ when it was allowed to float at $Q = 0.0438$ Å^{-1}. More generally, the internal dynamics could be described as Rouse behaviour, which requires $\beta = 1/2$.[49] The fits in **Figure 5** were made with $\beta = 1/2$ fixed for all Q, and with $A = 1$ for $Q = 0.0438$ Å^{-1}. For the four largest values of Q, the fitting revealed $A = 0$, i.e. there was a dominant contribution due to internal dynamics. The values of Γ extracted from these fits are shown in **Figure 6**. There is some scatter in the relaxation rate results, but it was possible to fit these data to **eqn 5**.

As an alternative to Rouse behaviour, a Zimm consideration of local chain motion[53] ($\beta = 2/3$) was tested and found to be unsuitable: although the data could be fitted to **eqn 4** with $\beta = 2/3$, there was no internal consistency in the results because the values of A calculated from **eqn 4** with $\beta = 2/3$ did not exhibit monotonic behaviour with increasing Q. The same applies to data obtained from samples measured at temperatures closer to the LCST (these results are included in the **ESI**), where fitting was possible, but internal consistency absent when fitted to both $\beta = 1/2$ and $\beta = 2/3$. This does not mean that Rouse dynamics do not apply to the polymers close to the collapse transition, but simply that, if it does, these experiments did not detect it.

The values of $D_0(Q = 0.0438$ Å$^{-1})$ are $(2.66\pm0.04) \times 10^{-11}$ m^2/s (25:1 at 15 °C) and $(3.83\pm0.08) \times 10^{-11}$ m^2/s (90:1 at 24 °C), and, by expressing the internal dynamics in terms of a diffusion coefficient, internal dynamics and translational diffusion can be compared. To do this, **eqn 5** is simplified to $\Gamma = D_R b^2 Q^4/2$, which allows a determination of D_R (where $D_R = k_B T/\zeta$). For the respective HB-PNIPAM samples (25:1 at 15 °C and 90:1 at 24 °C), $D_R = (8.4\pm0.6) \times 10^{-12}$ m^2/s and $(1.3\pm0.1) \times 10^{-11}$ m^2/s for the respective HB-PNIPAM. The value of the Kuhn length used here was $b = 0.7$ nm,[54] but a range of values has been reported, from below[55, 56] 0.5 nm to 1.0 nm.[57] (These possible discrepancies were not applied to the uncertainty in D_R.) The values of D_R are a factor of three smaller than D_0, which is likely to be due to the shape of the hyperbranched polymers as well as the longest relaxation time in Rouse dynamics being longer than that for equivalent Zimm dynamics.[38] It is nevertheless perhaps still surprising that the translational motion is more rapid than local motion, which suggests that local motion of branches in the hyperbranched polymer cannot be treated as if neighbouring branches did not interact

with each other. Dynamic laser-light scattering experiments have shown that PNIPAM microgels exhibit faster internal motion compared to that of the whole polymer,[58] but these were for very high molar mass materials (2.2×10^8 g/mol) and it is possible that for smaller microgels, but with similar crosslinking density (approximately 60 monomers per crosslink),[59] that the internal motion would be unchanged whilst translational motion increased. Comparable measurements for highly-branched polymers are lacking, but spin-echo (DOSY) NMR has been used to measure the (translational) diffusion of HB-PNIPAM created from a polyamidoamine hyperbranched core, with a number average molar mass of 192 kg/mol and a branching ratio of ~70 at 25 °C to yield a diffusion coefficient of 4×10^{-11} m^2/s,[60] in excellent agreement with $D_0 = 3.8 \times 10^{-11}$ m^2/s obtained from the NSE data (90:1 at 24 °C).

Local chain motion can be compared with NSE data from PNIPAM gels, whereby both ends of network strands are tethered by permanent crosslinks. Here, experiments have been performed on macroscopic gels[61] and microgels.[52, 62] Macroscopic and microscopic gels with the same crosslinking density were observed to have very similar local dynamics,[62] but there have been differences between microgels where the gel is rigid (significant crosslinking) and $\beta = 1$ is observed,[62] or microgels with fewer crosslinks, which follow Zimm behaviour.[52] Both of these example contrast with the highly-branched polymers discussed in the present work for which local motion is described well by Rouse behaviour.

Conclusions

SANS experiments show that below LCST the generalized Zimm equation (**eqn 1**) at small Q describes the structure of both highly-branched and linear poly(N-isopropylacrylamide) in terms of a single length scale (correlation length). The fractal dimension increases for HB-PNIPAM as the LCST is reached indicating a collapse in the polymer structure although that of the linear PNIPAM remains for an expanded coil in good solvent. Above the LCST the HB-PNIPAM forms particles with a radius that increases with increasing temperature. The SANS data for these particles were successfully fitted to a disperse sphere model. Linear PNIPAM formed large particles above the LCST, although a temperature dependence was not obtained.

A combination of both translational and local motions was probed by NSE and it was observed that the translational diffusion was faster than that associated with local dynamical motion. The data from the local (internal) dynamics of the HB-polymers however could only be explained by Rouse behaviour.

Because hyperbranched polymers cannot entangle with each other under good solvent conditions, their solution dynamics can test differences in polymer behaviour with that of linear polymers. HB-PNIPAM exhibits structural behaviour that changes with temperature and, unlike linear PNIPAM, its LCST transition is not particularly sharp. Internal dynamics are not influenced by hydrodynamic effects and translational diffusion is relatively rapid. Above the LCST, the polymers start to

Soft Matter

aggregate forming structures which increase in size with temperature. The shape of these structures is not uniform; there is substantial dispersity in size, which may reflect the large dispersities in the molar mass of the individual HB-PNIPAM structures.

Conflicts of interest

There are no conflicts to declare.

Acknowledgements

Notes and references

1. J. A. Alfurhood, P. R. Bachler and B. S. Sumerlin, *Polym. Chem.*, 2016, **7**, 3361-3369.
2. R. M. England and S. Rimmer, *Polym. Chem.*, 2010, **1**, 1533-1544.
3. C. J. Hawker, P. J. Farrington, M. E. MacKay, K. L. Wooley and J. M. J. Fréchet, *J. Am. Chem. Soc.*, 1995, **117**, 4409-4410.
4. M. Jikei and M. Kakimoto, *Prog. Polym. Sci.*, 2001, **26**, 1233-1285.
5. E. Malmström and A. Hult, *J. Macromol. Sci. C: Polym. Rev.*, 1997, **37**, 555-579.
6. B. I. Voit, *C. R. Chim.*, 2003, **6**, 821-832.
7. Y. Zheng, S. Li, Z. Weng and C. Gao, *Chem. Soc. Rev.*, 2015, **44**, 4091-4130.
8. T. J. Prosa, B. J. Bauer, E. J. Amis, D. A. Tomalia and R. Scherrenberg, *J. Polym. Sci. B: Polym. Phys.*, 1997, **35**, 2913-2924.
9. B. I. Voit and A. Lederer, *Chem. Rev.*, 2009, **109**, 5924-5973.
10. A. Blumen, A. Jurjiu and T. Koslowski, *Macromol. Symp.*, 2004, **210**, 301-310.
11. D. M. A. Buzza, *Eur. Phys. J. E*, 2004, **13**, 79-86.
12. E. T. F. Geladé, B. Goderis, C. G. de Koster, N. Meijerink, R. A. T. M. van Benthem, R. Fokkens, N. M. M. Nibbering and K. Mortensen, *Macromolecules*, 2001, **34**, 3552-3558.
13. V. M. Garamus, T. V. Maksimova, H. Kautz, E. Barriau, H. Frey, U. Schlotterbeck, S. Mecking and W. Richtering, *Macromolecules*, 2004, **37**, 8394-8399.
14. Y. H. Kim, *J. Polym. Sci. A: Polym. Chem.*, 1998, **36**, 1685-1698.
15. E. Malmström, A. Hult, U. W. Gedde, F. Liu and R. H. Boyd, *Polymer*, 1997, **38**, 4873-4879.
16. D. Wang, Y. Jin, X. Zhu and D. Yan, *Prog. Polym. Sci.*, 2017, **64**, 114-153.
17. H. G. Schild, *Prog. Polym. Sci.*, 1992, **17**, 163-249.
18. J. Collett, A. Crawford, P. V. Hatton, M. Geoghegan and S. Rimmer, *J. R. Soc. Interface*, 2007, **4**, 117-126.
19. M. A. Cooperstein and H. E. Canavan, *Langmuir*, 2010, **26**, 7695-7707.
20. M. Krishnamoorthy, S. Hakobyan, M. Ramstedt and J. E. Gautrot, *Chem. Rev.*, 2014, **114**, 10976-11026.
21. K. Mandal, M. Balland and L. Bureau, *PLoS One*, 2012, **7**, e37548.
22. K. Uto, H. H. Tsui, C. A. DeForest and D.-H. Kim, *Prog. Polym. Sci.*, 2017, **65**, 53-82.
23. T. Wei, Z. Tang, Q. Yu and H. Chen, *ACS Appl. Mater. Interfaces*, 2017, **9**, 37511-37523.
24. S. Hopkins, S. R. Carter, J. W. Haycock, N. J. Fullwood, S. MacNeil and S. Rimmer, *Soft Matter*, 2009, **5**, 4928-4937.
25. J. Shepherd, P. Sarker, K. Swindells, I. Douglas, S. MacNeil, L. Swanson and S. Rimmer, *J. Am. Chem. Soc.*, 2010, **132**, 1736-1737.
26. S. Carter, B. Hunt and S. Rimmer, *Macromolecules*, 2005, **38**, 4595-4603.
27. S. Rimmer, S. Carter, R. Rutkaite, J. W. Haycock and L. Swanson, *Soft Matter*, 2007, **3**, 971-973.
28. R. K. Heenan, J. Penfold and S. M. King, *J. Appl. Crystallogr.*, 1997, **30**, 1140-1147.
29. S. M. King, in *Modern Techniques for polymer characterisation*, eds. R. A. Pethrick and J. V. Dawkins, Wiley, Chichester, 1999, pp. 171-232.
30. P. Schleger, G. Ehlers, A. Kollmar, B. Alefeld, J. F. Barthelemy, H. Casalta, B. Farago, P. Giraud, C. Hayes, C. Lartigue, F. Mezei and D. Richter, *Physica B*, 1999, **266**, 49-55.
31. X. Li, H. ShamsiJazeyi, S. L. Pesek, A. Agrawal, B. Hammouda and R. Verduzco, *Soft Matter*, 2014, **10**, 2008-2015.
32. W. Burchard, *Macromolecules*, 1977, **10**, 919-927.
33. D. R. Vollet, D. A. Donatti, C. M. Awano, W. Chiappim Jr, M. R. Vicelli and A. Ibañez Ruiz, *J. Appl. Crystallogr.*, 2010, **43**, 1005-1011.
34. E. De Luca, R. W. Richards, I. Grillo and S. M. King, *J. Polym. Sci. B: Polym. Phys.*, 2003, **41**, 1352-1361.
35. G. ten Brinke and G. Hadziioannou, *Macromolecules*, 1987, **20**, 480-485.
36. K. N. Plunkett, X. Zhu, J. S. Moore and D. E. Leckband, *Langmuir*, 2006, **22**, 4259-4266.
37. X. Zhu, C. Yan, F. M. Winnik and D. Leckband, *Langmuir*, 2007, **23**, 162-169.
38. M. Rubinstein and R. H. Colby, *Polymer Physics*, Oxford University Press, Oxford, 2003.
39. M. Delsanti, J. P. Munch, D. Durand, J. P. Busnel and M. Adam, *Europhys. Lett.*, 1990, **13**, 697-702.
40. T. C. Lubensky and J. Isaacson, *Phys. Rev. A*, 1979, **20**, 2130-2146.
41. B. H. Zimm and W. H. Stockmayer, *J. Chem. Phys.*, 1949, **17**, 1301-1314.
42. P.-G. de Gennes, *Scaling Concepts in Polymer Physics*, Cornell University Press, Ithaca, 1979.
43. T. Cosgrove, P. C. Griffiths and P. M. Lloyd, *Langmuir*, 1995, **11**, 1457-1463.
44. H. M. Crowther, B. R. Saunders, S. J. Mears, T. Cosgrove, B. Vincent, S. M. King and G.-E. Yu, *Colloids Surf. A*, 1999, **152**, 327-333.
45. K. Kratz, T. Hellweg and W. Eimer, *Polymer*, 2001, **42**, 6631-6639.

46.   P. Wong, *Phys. Rev. B*, 1985, **32**, 7417-7424.
47.   S. Kunamaneni, D. M. A. Buzza, D. J. Read, D. Parker, A. M. Kenwright, W. J. Feast and A. L. Larsen, *Macromolecules*, 2006, **39**, 6720-6736.
48.   D. Richter, B. Ewen, B. Farago and T. Wagner, *Phys. Rev. Lett.*, 1989, **62**, 2140-2143.
49.   D. Richter, M. Monkenbusch, A. Arbe and J. Colmenero, *Adv. Polym. Sci.*, 2005, **174**, 1-221.
50.   L. R. Arriaga, I. López-Montero, G. Orts-Gil, B. Farago, T. Hellweg and F. Monroy, *Phys. Rev. E*, 2009, **80**, 031908.
51.   T. Hellweg and D. Langevin, *Phys. Rev. E*, 1998, **57**, 6825-6834.
52.   C. Scherzinger, O. Holderer, D. Richter and W. Richtering, *Phys. Chem. Chem. Phys.*, 2012, **14**, 2762-2768.
53.   M. Monkenbusch, in *Neutron Spin Echo Spectroscopy*, eds. F. Mezei, C. Pappas and T. Gutberlet, Springer, Berlin, 2003, pp. 246-267.
54.   W. Zhang, S. Zou, C. Wang and X. Zhang, *J. Phys. Chem. B*, 2000, **104**, 10258-10264.
55.   S. Cui, X. Pang, S. Zhang, Y. Yu, H. Ma and X. Zhang, *Langmuir*, 2012, **28**, 5151-5157.
56.   X. Ye, Y. Lu, L. Shen, Y. Ding, S. Liu, G. Zhang and C. Wu, *Macromolecules*, 2007, **40**, 4750-4752.
57.   E. Kutnyanszky, A. Embrechts, M. A. Hempenius and G. J. Vancso, *Chem. Phys. Lett.*, 2012, **535**, 126-130.
58.   C. Wu and S. Zhou, *Macromolecules*, 1996, **29**, 1574-1578.
59.   C. Wu and S. Zhou, *Macromolecules*, 1997, **30**, 574-576.
60.   H. H. Nguyen, B. Payré, J. Fitremann, N. Lauth-de Viguerie and J. D. Marty, *Langmuir*, 2015, **31**, 4761-4768.
61.   S. Koizumi, M. Monkenbusch, D. Richter, D. Schwahn and B. Farago, *J. Chem. Phys.*, 2004, **121**, 12721-12731.
62.   Y. Hertle, M. Zeiser, P. Fouquet, M. Maccarini and T. Hellweg, *Z. Phys. Chem.*, 2014, **228**, 1053-1075.